Inorganic Chemistry

Article

pubs.acs.org/IC

Exploring the Color of Transition Metal Ions in Irregular Coordination Geometries: New Colored Inorganic Oxides Based on the Spiroffite Structure, $Zn_{2-x}M_xTe_3O_8$ (M = Co, Ni, Cu)

S. Tamilarasan,[†] Debajit Sarma,[†] S. Bhattacharjee,[‡] U. V. Waghmare,*[,‡] S. Natarajan,[†] and J. Gopalakrishnan*[,†]

[†]Solid State and Structural Chemistry Unit, Indian Institute of Science, Bangalore-560012, India

[‡]Theoretical Sciences Unit, Jawaharlal Nehru Centre for Advanced Scientific Research, Jakkur P.O., Bangalore-560064, India

Supporting Information

ABSTRACT: We describe the synthesis, crystal structures, and optical absorption spectra of transition metal-substituted spiroffite derivatives, $Zn_{2-x}M_xTe_3O_8$ (M^{II} = Co, Ni, Cu; $0 < x \leq 1.0$). The oxides are readily synthesized by solid state reaction of stoichiometric mixtures of the constituent binaries at 620 °C. Reitveld refinement of the crystal structures from powder X-ray diffraction (XRD) data shows that the Zn/MO_6 octahedra are strongly distorted, as in the parent $Zn_2Te_3O_8$ structure, consisting of five relatively short Zn/M^{II}−O bonds (1.898−2.236 Å) and one longer Zn/M^{II}−O bond (2.356−2.519 Å). We have interpreted the unique colors and the optical absorption/diffuse reflectance spectra of $Zn_{2-x}M_xTe_3O_8$ in the visible, in terms of the observed/irregular coordination geometry of the Zn/M^{II}−O chromophores. We could not however prepare the fully substituted $M_2Te_3O_8$ (M^{II} = Co, Ni, Cu) by the direct solid state reaction method. Density Functional Theory (DFT) modeling of the electronic structure of both the parent and the transition metal substituted derivatives provides new insights into the bonding and the role of transition metals toward the origin of color in these materials. We believe that transition metal substituted spiroffites $Zn_{2-x}M_xTe_3O_8$ reported here suggest new directions for the development of colored inorganic materials/pigments featuring irregular/distorted oxygen coordination polyhedra around transition metal ions.

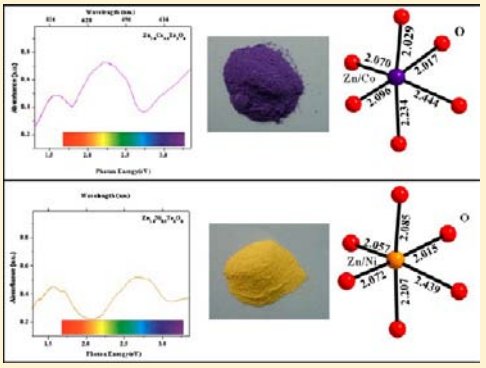

INTRODUCTION

Inorganic solids displaying brilliant colors have remained fascinating objects of attraction for ages.[1] Thus, gemstones such as red ruby, green emerald, blue sapphire, and the blue−green turquoise, and pigment materials such as Egyptian blue ($CoCuSi_4O_{10}$), Cobalt blue ($CoAl_2O_4$), Cadmium yellow (CdS), and Vermilion red (HgS) are some of the well-known inorganic solids of both scientific/technological as well as aesthetic/artistic interest. The causes of colors in solids have been widely explored and well documented from a scientific standpoint.[2,3] Although fifteen different causes of color in substances have been identified,[2] insofar as inorganic solids where color originates from a transition metal ion is concerned, optical absorption in the visible region (380−740 nm) arising from ligand field effects around the transition metal ion and intervalence charge−transfer between two atoms in inorganic hosts appear to be the two major causes of color.

While the colors of transition metal ions in symmetric/regular ligand fields, namely, octahedral and tetrahedral geometries, obtaining in several inorganic host materials are well-known,[2−4] colors of metal ions in irregular/less symmetric ligand fields is a topic of relatively recent interest, that is providing rich dividends for the development of new inorganic colored materials. Thus, trigonal bipyramidal geometry for transition metal ions such as Mn(III) and Fe(III) in $YInO_3$ and related hosts results in brilliant blue and orange colors respectively,[5,6] and Co(II) in distorted trigonal bipyramidal and octahedral geometries in $ZnMoO_4$ gives rise to a new blue pigment material,[7] while square pyramidal geometry around Cu(II) in $R_2Cu_2O_5$ and R_2BaCuO_5 (R = rare earth) produces intense green/bluish−green materials of pigment quality.[8] Similarly, 3d-transition metal ions doped into distorted octahedral coordination geometries, as obtaining in tialite (Al_2TiO_5),[9] pseudobrookite (Fe_2TiO_5),[10] and karrooite ($MgTi_2O_5$)[11] have given rise to several new ceramic pigments.[9−11]

Continuing our efforts to explore and develop new colored inorganic solids containing transition metal ions in unusual oxidation states[12] or in unusual/irregular coordination geometries,[13] we have explored the formation of colored materials by doping 3d metal ions in a novel host, $Zn_2Te_3O_8$, crystallizing in the spiroffite structure.[14] Both Zn(II) and Te(IV) occur in distorted/irregular coordination geometries in this structure.[15,16] The oxygen coordination of Zn(II) is essentially five-fold (trigonal bipyramidal) with bond distances ranging

Received: November 22, 2012
Published: May 9, 2013

   dx.doi.org/10.1021/ic302557j | Inorg. Chem. 2013, 52, 5757−5763

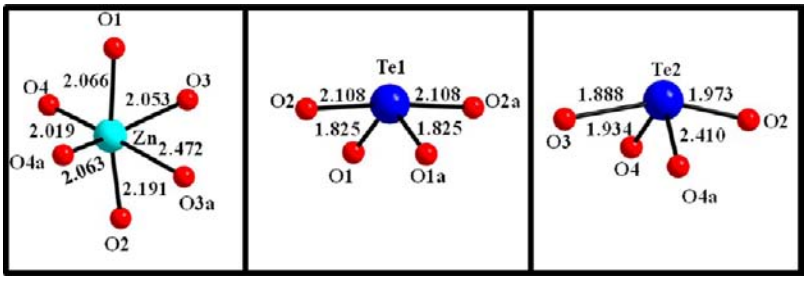

Figure 1. Irregular coordination geometries of ZnO_6 and TeO_4 polyhedra in $Zn_2Te_3O_8$.

from 2.019−2.191 Å (the sixth bond to oxygen being at 2.472 Å), while Te(IV) occurs in two asymmetric four−fold coordinations (Figure 1). We believed that doping divalent 3d metal ions at the Zn(II) site would give rise to novel colored materials that would reflect the distorted octahedral/five-fold coordination geometry of Zn(II) in this host. Our efforts have identified new colored solids for Co(II) (purple), Ni(II) (yellow), and Cu(II) (parrot green) doping in this host. We describe the synthesis, structure, optical, and color characterization of these materials in this paper.

EXPERIMENTAL SECTION

Synthesis and Characterization. The $Zn_{2-x}M_xTe_3O_8$ oxides (M^{II} = Co, Ni, and Cu; $0 < x \leq 1$) were prepared by the conventional ceramic method. For this purpose, high purity ZnO, TeO_2, $MC_2O_4{\cdot}2H_2O$ (M = Co and Ni) and CuO were mixed in stoichiometric proportions, and the mixtures heated at 620 °C for 12 h with a grinding in between. Examination of the products by Powder X-ray Diffraction (PXRD) revealed the formation of nearly single phase materials for $Zn_{2-x}M_xTe_3O_8$ (M = Co, Ni, and Cu; $0 < x \leq 1$).

All oxides were characterized by PXRD, Scanning Electron Microscopy (SEM), and Energy-dispersive X-ray Spectroscopy (EDX). PXRD patterns were recorded with a Philips X'pert Diffractometer (Ni-filtered Cu Kα radiation, λ = 1.5418 Å). PXRD data for Rietveld refinement of the structures were collected at room temperature employing the same diffractometer (Philips X'pert Diffractometer, Ni-filtered Cu Kα radiation, λ = 1.5418 Å) in the 2θ range 5−100° with a step size of 0.03° and step duration 50 s. About 100 mg of the powdered samples were tightly packed in a rectangular sample holder (1 × 2 cm) for recording the PXRD data.

The structure of representative members were refined from PXRD data employing the program GSAS.[17] All the 18 general positions were refined. A second order shifted Chebyschev polynomial for the background, zero, LP factor, scale, pseudo-Voigt profile function (U, V, W, and X), lattice parameters, atomic parameters, and U_{iso} (total 39 parameters) were used in refinement. The thermal parameters were constrained to be the same for atoms occupying the same site (Zn and M^{II}).

The diffuse reflectance spectra for all the powdered samples were recorded on a Perkin-Elmer Lambda 35 UV−vis double beam spectrometer over the spectral region of 200−900 nm. The diffuse reflectance data were converted to absorbance data employing the Kubelka−Munk function,

$$F(R) = (1 - R)^2/2R = K/S$$

where R denotes the reflectance, K and S represent absorption and scattering, respectively.

Room-temperature solid-state emission and excitation spectra were also recorded for all the samples (Perkin-Elmer, U.K. model no. LS55). For characterization of pigment quality of the samples, the CIE-1931 chromaticity coordinates were calculated using gocie.exe program from http://www.geocities.com/krjustin/gocie.html. SEM and EDX data were recorded on a FEI ESEM Quanta 200 instrument.

We carried out electronic structure modeling based on first principles density functional theory (DFT) as implemented in the Quantum ESPRESSO package.[18] We used ultrasoft pseudopotentials to represent the interaction between ionic cores and valence electrons, and a generalized gradient approximation (GGA) to exchange correlation energy functional as parametrized by Perdew, Burke, and Ernzerhof (PBE). An energy cutoff of 30 Ry was employed to truncate the plane-wave basis used for representing Kohn−Sham wave functions and 150 Ry for that used to represent charge density. The crystal structures were determined using the Broyden−Fletcher−Goldfarb−Shanno (BFGS) method for minimization of energy until the Hellmann−Feynman forces on each atom were smaller than 0.03 eV/Å in magnitude. Integrations over the Brillouin zone was sampled with a 2 × 4 × 2 mesh of k-points in calculations of structural relaxation, and the density of states was determined with a finer, 6 × 12 × 6, mesh of k-points. Occupation numbers were smeared using the Fermi−Dirac distribution function with a temperature broadening of 0.003 Ry. For the doped compounds, we considered 12.5% substitution of Co, Ni, and Cu at Zn-sites.

RESULTS AND DISCUSSION

Synthesis and Structure. In an effort to explore the color of 3d-transition metal ions in the spiroffite $Zn_2Te_3O_8$ host, we investigated substitution of transition metal ions at both Zn^{II} and Te^{IV} sites. While we could readily substitute divalent Mn^{II}, Co^{II}, Ni^{II}, and Cu^{II} ions at the Zn^{II} sites to give $Zn_{2-x}M^{II}{}_xTe_3O_8$ (M^{II} = Mn, Co, Ni, Cu) for $0 < x \leq 1$, our efforts to prepare trivalent (Cr^{III}, Mn^{III}, and Fe^{III}) metal substituted derivatives, by the coupled substitution, $Zn^{II} + Te^{IV} \rightarrow M^{III} + Sb^{III}$, did not materialize. All the syntheses have been carried out by direct solid state reaction of the constituent binaries. We could obtain brilliantly colored $Zn_{2-x}M^{II}{}_xTe_3O_8$ for M^{II} = Co (purple), M^{II} = Ni (yellow) and M^{II} = Cu (parrot green), but for M^{II} = Mn, the samples were light beige in color. We focused our attention on the Co, Ni, and Cu compounds in this work.

PXRD together with SEM and EDX shows that $Zn_{2-x}M^{II}{}_xTe_3O_8$ (M^{II} = Mn, Co, Ni, Cu) are essentially single-phase solids isostructural with the parent $Zn_2Te_3O_8$ (Figure 2; Supporting Information, Figures S1−S4). We refined the crystal structures of $Zn_{2-x}M^{II}{}_xTe_3O_8$ members for M^{II} = Co, Ni, and Cu from PXRD data. We present the refinement data for a representative member $ZnCoTe_3O_8$ in Figure 3 and Table 1. The remaining refinement results are given as Supporting Information, Figures S5−S8 and Tables S1−S4. A summary of the crystal structure data together with corresponding data for the parent $M_2Te_3O_8$ (M = Zn, Co, Ni, and Cu) is given in Table 2.

The crystal structure of all the $Zn_{2-x}M^{II}{}_xTe_3O_8$ members is essentially similar to that of the parent spiroffite[14−16] showing edge shared octahedral M_2O_{10} dimers, which are interlinked through corners (Figure 4), wherein the Te^{IV} ions occupy irregular 4-fold coordination sites. A closer look at the

dx.doi.org/10.1021/ic302557j | Inorg. Chem. 2013, 52, 5757−5763

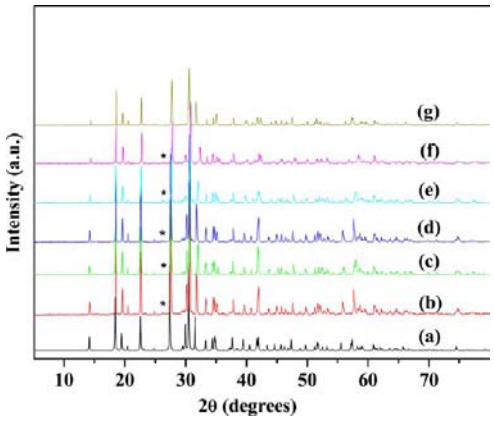

Figure 2. PXRD patterns of (a) $Zn_2Te_3O_8$, (b) $Zn_{1.8}Co_{0.2}Te_3O_8$, (c) $ZnCoTe_3O_8$, (d) $Zn_{1.8}Ni_{0.2}Te_3O_8$, (e) $Zn_{1.5}Ni_{0.5}Te_3O_8$, (f) $ZnNiTe_3O_8$, and (g) $Zn_{1.8}Cu_{0.2}Te_3O_8$. The asterisk (*) denotes a minor impurity of TeO_2.

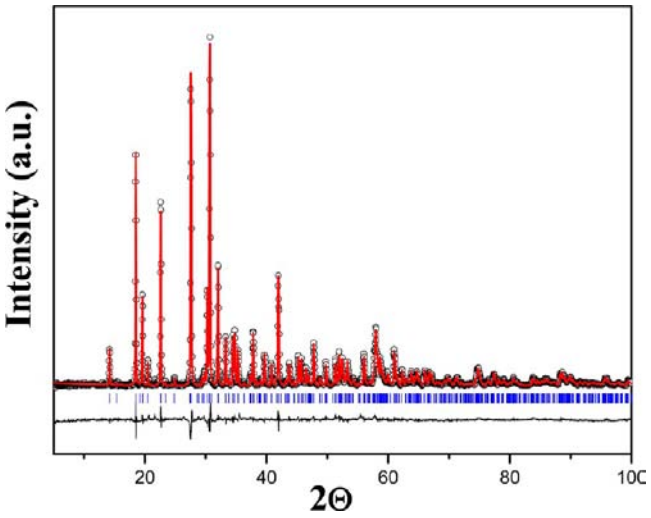

Figure 3. Rietveld refinement of the structure of $ZnCoTe_3O_8$ from powder XRD data, showing observed (○), calculated (red solid lines) and difference (bottom) profiles.

structural data however reveals subtle variations in the coordination geometries around Zn/M ions. In all the cases Zn/M-O_6 polyhedron is irregular, consisting of five relatively short and one long Zn/M−O bonds. The octahedral bond length distortion, quantified in terms of the distortion parameter Δ (Table 2), remains essentially the same or even slightly increases for M = Ni, Cu as compared to parent $Zn_2Te_3O_8$. A comparison of the Δ values for the end members $M_2Te_3O_8$ (M = Co, Ni, and Cu) from the literature[16] shows that for M = Co and Ni compounds, the MO_6 octahedra become more regular, while Cu shows a pronounced distortion because one of the Cu−O bond is unusually long (2.782 Å).

In an effort to identify whether the Zn/M-O_6 polyhedra are to be regarded as irregular octahedra or trigonal-bipyramidal, we considered both the Zn/M−O bond valence sums (BVS) as well as actual bond lengths and bond angles. While conceding that BVS data are not of quantitative significance especially when different atoms occupy the same site and local relaxations are unknown, we made use of the data to figure out the approximate geometry of the Zn/M-O_6 polyhedra in the spiroffite solid solutions. When we consider only the five short Zn/M−O bonds, we arrived at a bond valence sums (BVS) of approximately 1.80 to 1.85, the long Zn/M−O bond contributing only around 0.15 for the valence. However, when we consider all the six bonds, the BVS values are close to the expected 2.0 (Table 2). Accordingly, we concluded that the Zn/M-O_6 polyhedra are to be regarded as octahedra rather than trigonal biprymids, although the actual bond lengths and bond angles (Figure 3) indicate that the octahedra are far from ideal, being heavily distorted. Accordingly, we interpret in the next section the color and optical absorption spectra of these compounds as arising from heavily distorted octahedral Zn/M-O_6 chromophores.

Color and Optical Properties. In Figure 5, we show the color of $Zn_{2-x}M^{II}_xTe_3O_8$ as seen in daylight and the corresponding optical absorption spectra of the Co, Ni, and Cu compounds in the visible region in Figures 6−8 respectively. The spectra of the Co-compounds display essentially two absorption maxima centered around 1.60 and 2.25 eV photon energies. Both the bands are relatively broad and strong. The band centered at 2.25 eV shows a lower energy (2.0 eV) and a higher energy shoulder (2.45 eV). $Co^{II}O_6$ undistorted octahedral chromophore[4] typically shows a near IR absorption around 1 eV due to $^4T_{1g} \rightarrow {}^4T_{2g}$ and a broad visible absorption spreading over 2 to 3 eV with a maximum around 2.5 eV which corresponds to $^4T_{1g} \rightarrow {}^4T_{1g}(P)$ and $^4T_{1g} \rightarrow {}^4A_{2g}$, the latter often occurring as a shoulder. On the other hand, the CoO_5 trigonal-bipyramidal chromophore shows three absorp-

Table 1. Crystallographic Data for $ZnCoTe_3O_8$[a]

atom	site	*x*	*y*	*z*	U_{iso}(Å^2)	occupancy
Zn	8f	0.229(1)	0.296(1)	0.348(1)	0.016(1)	0.48(3)
Co	8f	0.229(1)	0.296(1)	0.348(1)	0.016(1)	0.52(2)
Te(1)	4e	0	0.352(1)	0.75	0.020(1)	1
Te(2)	8f	0.136(1)	0.692(1)	0.555(1)	0.017(1)	1
O(1)	8f	0.077(1)	0.402(2)	0.355(1)	0.038(6)	1
O(2)	8f	0.109(1)	0.377(2)	0.635(1)	0.011(5)	1
O(3)	8f	0.232(1)	0	0.446(1)	0.013(5)	1
O(4)	8f	0.192(1)	0.885(2)	0.689(1)	0.011(5)	1

[a]Space group *C*2/*c*: *a* = 12.684(1) Å, *b* = 5.208(1) Å, *c* = 11.706(1) Å, *β* = 99.25(1); *V* = 763.22 Å^3. Reliability Factors (%): R_p = 4.83, R_{wp} = 6.27, χ^2 = 3.98, R_F^2 = 8.94. Bond Lengths (Å): Zn/Co−O(1) = 2.008(1), Zn/Co−O(2) = 2.216(1), Zn/Co O(3) = 2.062(1), Zn/Co−O(3) = 2.397(1), Zn/Co−O(4) = 2.078(1), Zn/Co −O(4) = 2.020(1); ⟨Zn/Co−O⟩ = 2.130. (2) Te(1)−O(1) = 1.933(1), (2) Te(1)−O(2) = 2.085(1); ⟨Te(1)−O⟩ = 2.009. Te(2)−O(1) = 2.789(1), Te(2)−O(2) = 1.949(1), Te(2)−O(3) = 2.356(1), Te(2)−O(3) = 1.991(1), Te(2)−O(4) = 1.899(1); ⟨Te(2)−O⟩ = 2.197. Bond valence sums: Zn/Co = 1.98 (expected 2), Bond valence sums: Zn = 1.83 (expected 2), (5-coordinated). Contribution of the long bond =0.15Te(1) = 3.75 (expected 4), Te(2) = 3.75 (expected 4).

dx.doi.org/10.1021/ic302557j | *Inorg. Chem.* 2013, 52, 5757−5763

Table 2. Summary of Crystal Structure Data of $Zn_{1-x}M^{II}{}_xTe_3O_8$ ($C2/c$) (M = Co, Ni, and Cu)

compound	a (Å)	b (Å)	c (Å)	β (deg)	V (Å^3)	BVS (5/6)[b]	Δ[c]
$Zn_{1.8}Co_{0.2}Te_3O_8$	12.679(1)	5.200(1)	11.767(1)	99.53(1)	765.10	1.80/1.92	4.88
$ZnCoTe_3O_8$	12.684(1)	5.208(1)	11.706(1)	99.25(1)	763.22	1.83/1.98	4.15
$Zn_{1.8}Ni_{0.2}Te_3O_8$	12.643(1)	5.202(1)	11.754(1)	99.45(1)	762.65	1.78/1.91	4.48
$Zn_{1.5}Ni_{0.5}Te_3O_8$	12.592(1)	5.209(1)	11.710(1)	99.23(1)	758.23	1.80/1.92	4.19
$ZnNiTe_3O_8$	12.519(1)	5.216(1)	11.625(1)	98.92(1)	749.95	1.90/2.06	5.80
$Zn_{1.8}Cu_{0.2}Te_3O_8$	12.567(1)	5.208(1)	11.846(1)	99.62(1)	764.40	1.82/1.93	6.56
$Zn_2Te_3O_8$[a]	12.681(2)	5.200(2)	11.786(2)	99.60(1)	766.3	1.84/1.97	5.31
$Co_2Te_3O_8$[a]	12.690(1)	5.211(2)	11.632(2)	98.98(1)	759.7	1.73/1.92	1.99
$Ni_2Te_3O_8$[a]	11.407(1)	5.207(1)	11.509(1)	98.73(1)	735.0	1.67/1.91	1.31
$Cu_2Te_3O_8$[a]	11.837(1)	5.266(2)	12.242(1)	100.31(1)	750.7	1.97/2.02	18.24

[a]For comparison the data for the parent $M^{II}{}_2Te_3O_8$ taken from the literature (ref 15 16,) are given. [b]Bond valence sums (BVS) are given for both five short and all the six bonds around $Zn/M^{II}O_6$ polyhedra. [c]Δ is the polyhedral distortion parameter defined by $\Delta = 1/N\Sigma [\{(r - \langle r\rangle)/\langle r\rangle\}^2]10^3$; where N is the number of bonds.

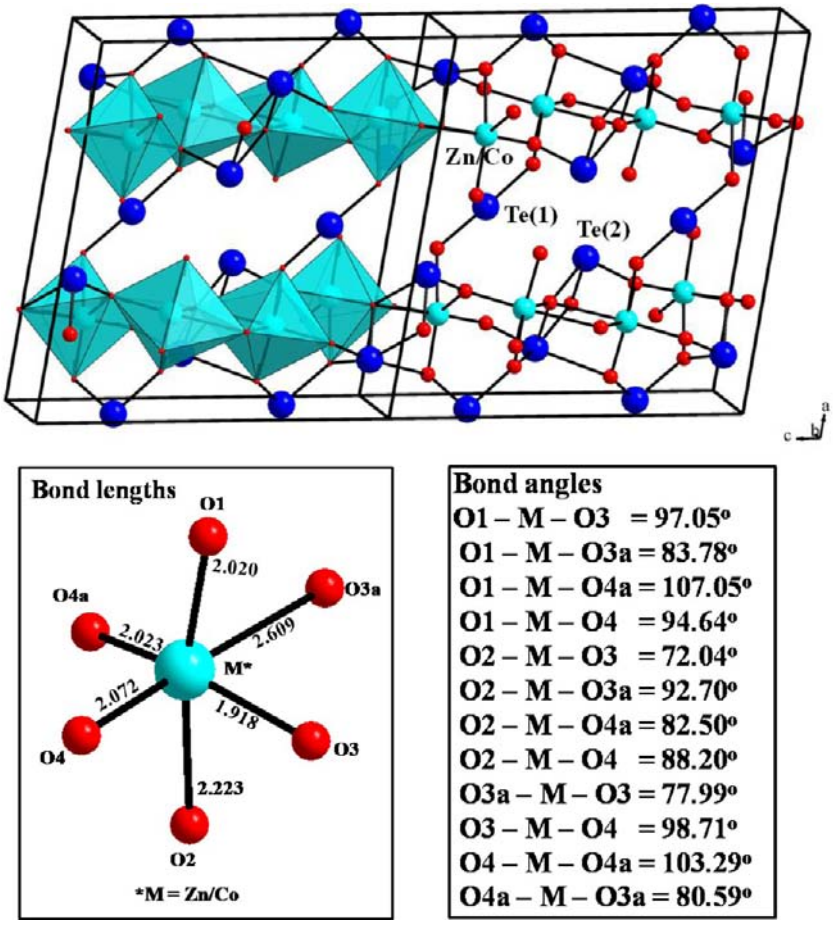

Figure 4. Crystal structure of $ZnCoTe_3O_8$ drawn from the data given in Figure 3 and Table 1. The bond lengths and bond angles of the $Zn/Co-O_6$ polyhedron are shown in the bottom panels.

tion bands centered around 1.35, 2.0, and 2.5 eV in the visible region.[4,19] Accordingly we see that the spectra of spiroffite $Zn_{2-x}Co^{II}{}_xTe_3O_8$ (Figure 6) corresponds to neither CoO_6 (regular octahedral) nor CoO_5 (trigonal bipyramidal) chromophores. The spectra observed therefore are a manifestation of the distorted/irregular Zn/CoO_6 chromophore. While a definite assignment of the absorption bands is difficult, the bands could be assigned approximately as corresponding to the $^4T_{1g} \rightarrow {}^4T_{1g}(P)$ (2.25 eV) and $^4T_{1g} \rightarrow {}^4A_{2g}$ (1.6 eV) transitions for an undistorted CoO_6 chromophore. Presumably, the low symmetry/distorted $Zn/Co^{II}O_6$ chromophore imparts a brilliant purple color which arises from the two valleys of low absorption centered around 2.8 eV (blue) and 1.8 eV (red) in the spectra of $Zn_{2-x}Co^{II}{}_xTe_3O_8$ (Figure 6). It is known that in general low symmetry component of the ligand field enhances absorption intensity as well as results in band splitting.[4]

The spectra of $Zn_{2-x}Ni^{II}{}_xTe_3O_8$ compounds (Figure 7) show two broad absorptions in the visible centered around 2.75 and 1.60 eV with a deep valley of no absorption around 2.10 eV, the latter imparting a yellow color to the materials. Typical octahedral NiO_6 chromophores as occur in Ni^{II} salts and Ni^{2+} doped MgO display a broad absorption spreading between 1.5

dx.doi.org/10.1021/ic302557j | Inorg. Chem. 2013, 52, 5757−5763

Figure 5. Color of $Zn_{2-x}M_xTe_3O_8$ oxides for various values of x as seen in the daylight.

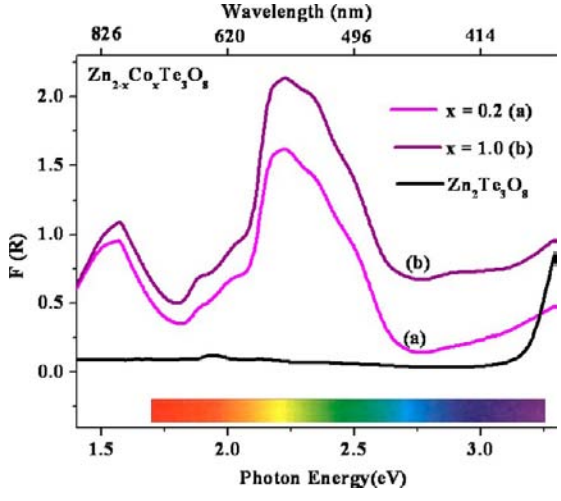

Figure 6. Diffuse reflectance spectra of $Zn_{2-x}Co_xTe_3O_8$ oxides. $F(R)$ is the Kubelka–Munk function.

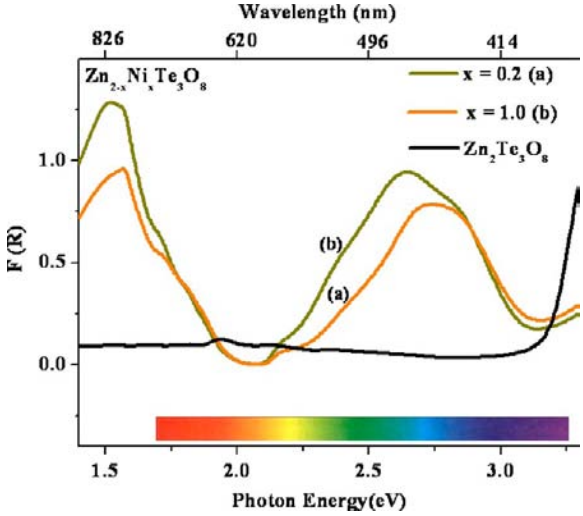

Figure 7. Diffuse reflectance spectra of $Zn_{2-x}Ni_xTe_3O_8$ oxides. $F(R)$ is the Kubelka–Munk function.

and 2.2 eV with a doublet maxima at around 1.75 and 1.90 eV (attributed to $^3A_{2g} \rightarrow {}^3T_{1g}$; $^3A_{2g} \rightarrow {}^1E_g$ transitions) which give a greenish color to the material.[4,19] Accordingly, the spectrum of $Zn_{2-x}Ni^{II}{}_xTe_3O_8$ is not typical of a regular NiO_6 octahedral chromophore. Also it is not similar to the NiO_5 trigonal bipyramidal chromophore.[19] Therefore, both the color and optical absorption spectra of $Zn_{2-x}Ni^{II}{}_xTe_3O_8$ are unique and distinct from the regular octahedral and trigonal bipyramidal $Ni^{II}O_6$ and $Ni^{II}O_5$ chromophores, reflecting the distorted octahedral NiO_6 in the host.

The spectra of $Zn_{2-x}Cu^{II}{}_xTe_3O_8$ (Figure 8) shows a maximum near the red end (1.6 eV) of the visible spectrum and an absorption in the blue that continues in the UV region, leaving a shallow valley of low absorption between 2 to 2.5 eV. This unique spectral feature which imparts a parrot green color to these materials is different from the optical absorption

dx.doi.org/10.1021/ic302557j | Inorg. Chem. 2013, 52, 5757–5763

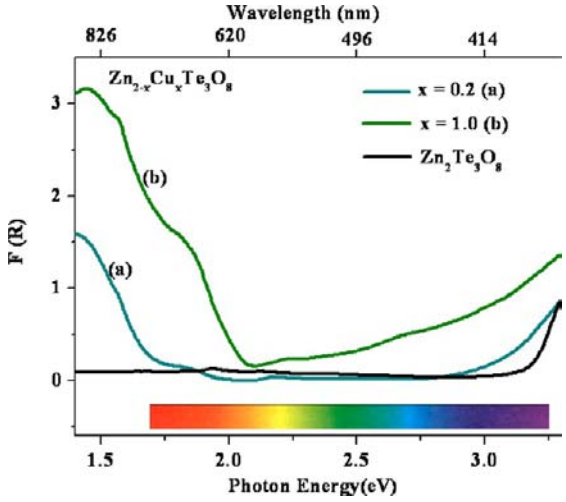

Figure 8. Diffuse reflectance spectra of $Zn_{2-x}Cu_xTe_3O_8$ oxides. $F(R)$ is the Kubelka–Munk function.

spectra of Jahn–Teller distorted CuO_6 chromophores as obtaining in $CuSO_4{\cdot}5H_2O$[20] and Cu^{2+} in MgO.[21] CuO_6 chromophores show a broad absorption around 1.60 eV (due to the ligand field $^2E_{2g} \rightarrow {}^2T_{2g}$ transition) and a sharp/strong absorption edge/band beyond the visible, greater than 3.5 eV, leaving a valley of low absorption in the entire visible between 3.25 to 2 eV giving a pale blue color. In contrast, the spectra of $Zn_{2-x}Cu^{II}{}_xTe_3O_8$ show a strong absorption starting from 2.5 eV extending into the UV (which could be due to a charge transfer between O^{2-} and Cu^{2+}). This onset of charge transfer at a relatively lower energy in $Zn_{2-x}Cu^{II}{}_xTe_3O_8$ as compared to other known CuO_6 chromophores referred to above renders the sample uniquely colored with a parrot green.

We tried to synthesize fully substituted $M^{II}{}_2Te_3O_8$ (M^{II} = Co, Ni, Cu) by direct solid state reaction of the binary constituents, but we failed in our attempts; we always obtained a mixture of various M–Te–O oxides, but not the spiroffite material. In the literature,[16] $M^{II}{}_2Te_3O_8$ have been synthesized by a hydrothermal method, which also did not yield 100% single phase spiroffite materials. When we compare our results on $Zn_{2-x}M^{II}{}_xTe_3O_8$ with the reported data on $M^{II}{}_2Te_3O_8$ for their colors and optical absorption spectra, we find that while the fully substituted $Co_2Te_3O_8$ (purple) and $Ni_2Te_3O_8$ (yellow) show color and absorption spectra similar to the corresponding $Zn_{2-x}M^{II}{}_xTe_3O_8$ (Co, Ni), $Cu_2Te_3O_8$ shows a different result: the latter having the largest distortion of the $Cu^{II}O_6$ chromophore (Δ = 18.24) is yellow showing a broad absorption peak at ~1.41 eV and the smallest band gap of 2.64 eV among this series of oxides.[16]

We carried out theoretical modeling of the electronic structures of the parent spiroffite as well as its substituted derivatives, $Zn_{2-x}M_xTe_3O_8$ (M = Ni, Cu) by DFT. The results and implications are described below.

Zn–O bond lengths (Supporting Information, Tables S6 and S7) in our optimized structure of $Zn_2Te_3O_8$ (ZTO) are in reasonable agreement with their experimental values.[15] Five of these bond lengths are comparable to those expected from the Shannon and Prewitt ionic radii in the ionic model, while the sixth one is much longer (2.56 Å), confirming the observed 5 + 1 coordination. The spread in the former from 2.02 to 2.18 Å hints at partial covalency of the Zn–O bonds. In the systems with M substituted at the Zn site, we find two types of changes in the M-O bond lengths: (a) Zn–O bond lengths are almost unchanged in the Co and Cu substituted compounds, while some of the short M-O bonds are even shorter (~ 1.97 Å) than the Zn–O bonds, and the long M-O bond is even longer (2.65 Å), and (b) the long Zn–O bond becomes even shorter (2.49 Å) in the Ni-substituted compound, and the long Ni–O bond is noticeably shorter (2.24 Å). Overall reduction in the M-O bonds upon the TM substitution is consistent with the M-O bond-lengths expected from the Shannon–Prewitt radii (Co–O = 2.01 Å, Ni–O = 2.05 Å, Cu–O = 2.09 Å).

The contrast in the structural changes with Co–Cu versus Ni substitution can be understood through the changes in electronic structure and Jahn–Teller arguments for the perfect MO_6 octahedral structure. To this end, we now examine the electronic density of states (DOS) and their projection on atomic orbitals (projected density of states, PDOS) of these compounds (see Figures 9 and 10 respectively). Our estimate

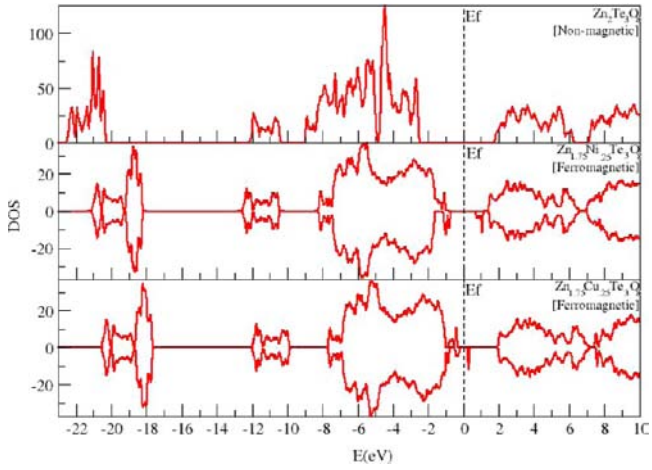

Figure 9. Electronic density of states (DOS) for $Zn_2Te_3O_8$ (ZTO), Ni and Cu substituted ZTO. The zero of the energy is set to the Fermi level.

of the band gap of ZTO is about 3.0 eV, and it is clear that its valence bands are mainly constituted of Zn-3d and oxygen 2p states (lower in energy), whereas its conduction band arises

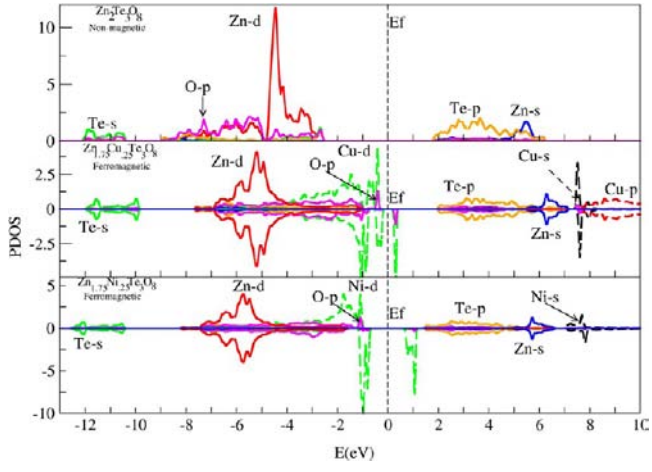

Figure 10. Projected density of states (PDOS) for $Zn_2Te_3O_8$ (ZTO), Ni and Cu substituted ZTO. The zero of the energy is set to the Fermi level.

dx.doi.org/10.1021/ic302557j | Inorg. Chem. 2013, 52, 5757–5763

from the Te-5p states and Zn-4s (higher in energy). Zn-3d and oxygen 2p states overlapping in the same energy range of the valence band confirms the partial covalent nature of the Zn−O bonding.

Upon Co, Ni, and Cu substitution, their partially filled d-states give rise to bands in the band gap of ZTO, effectively reducing the band gap (see Figure 10). Our calculations confirm the 2+ oxidation of state of each of them (d^7, d^8, d^9 configurations respectively) and reveal that the details of their structure involve crystal field and exchange splitting. It is easier to think of splitting of these d-states into sub-bands in terms of splitting in the ideal octahedral coordination as reference. The lowest energy t_{2g} and e_g states with up-spin are exchange split from those with down-spin, and are fully occupied. They couple strongly with oxygen 2p bands lifting them up in energy relative to the 3d-bands of Zn, and also giving rise to M-O covalency. In terms of the ideal octahedral symmetry, Cu^{2+} and Co^{2+} are Jahn−Teller active, while Ni^{2+} is passive, explaining the significantly distorted structure of the former and corresponding gaps between the down-spin d-sub-bands (see Figures 9 and 10). As a result, magnetic moments per M ion are 3, 2, and 1 μ_B for Co, Ni, and Cu, respectively. However, the gaps relevant to optical absorption involve electronic transitions between the d-states of M and p-states of oxygen or tellurium. Thus, the two absorption bands in Ni-substituted compounds are associated with its d-bands that are split widely due to the crystal field. In contrast, both exchange and crystal field splitting are weaker in Co and Cu substituted compounds giving rise to an essentially one absorption band below that of ZTO.

CONCLUSION

Transition metal substituted spiroffite type oxides, $Zn_{2-x}M^{II}_xTe_3O_8$ (M = Co, Ni, and Cu) reported herein are brilliantly colored materials (purple for Co^{II}, yellow for Ni^{II}, and parrot green for Cu^{II}) that could be of significance for the development of new inorganic pigments. Determination of crystal structure of these oxides from PXRD data has shown that the Zn/MO_6 chromophores are highly distorted from the octahedral symmetry, reflecting the ZnO_6 site in the parent $Zn_2Te_3O_8$. Investigation of the absorption spectra in the visible of these materials has shown that the unique colors, which are different from the regular octahedral $Co^{II}O_6$ and $Ni^{II}O_6$ and Jahn−Teller distorted $Cu^{II}O_6$ chromophores, arise from the distorted Zn/$M^{II}O_6$ chromophores in the $Zn_{2-x}M_xTe_3O_8$ (M = Co, Ni, Cu) spiroffites. DFT modeling of the electronic structure of both the parent and the substituted derivatives brings out the role of transition metals toward the origin of color in the $Zn_{2-x}M_xTe_3O_8$.

ASSOCIATED CONTENT

Supporting Information

SEM and EDX analysis, additional Rietveld refinement data, CIE chromaticity diagram and CIE coordinates. This material is available free of charge via the Internet at http://pubs.acs.org.

AUTHOR INFORMATION

Corresponding Author

*E-mail: gopal@sscu.iisc.ernet.in (J.G.), waghmare@jncasr.ac.in (U.V.W.).

Notes

The authors declare no competing financial interest.

ACKNOWLEDGMENTS

J.G. thanks the Indian National Science Academy, New Delhi, for the award of a Senior Scientist position. J.G. and S.N. thank the Department of Science and Technology, Government of India, for the award of Ramanna Fellowship.

REFERENCES

(1) Ball, P. *Bright Earth Art and the Invention of Color*; The University of Chicago Press: Chicago, IL, 2001.
(2) Nassau, K. *The Physics and Chemistry of Color*, 2nd ed; John Wiley: New York, 2001.
(3) Burns, R. G. *Mineralogical Applications of Crystal Field Theory*, 2nd ed; Cambridge University Press: Cambridge, U.K., 1993.
(4) Lever, A. B. P. *Inorganic Electronic Spectroscopy*; Elsevier: Amsterdam, The Netherlands, 1968.
(5) Smith, A. E.; Mizoguchi, H.; Delaney, K.; Spaldin, N. A.; Sleight, A. W.; Subramanian, M. A. *J. Am. Chem. Soc.* **2009**, *131*, 17084−17086.
(6) Jiang, P.; Li, J.; Sleight, A. W.; Subramanian, M. A. *Inorg. Chem.* **2011**, *50*, 5858−5860.
(7) Robertson, L.; Duttine, M.; Gaudon, M.; Demourgues, A. *Chem. Mater.* **2011**, *23*, 2419−2427.
(8) Kar, J. K.; Stevens, R.; Bowen, C. R. *J. Alloys Compd.* **2008**, *455*, 121−129.
(9) Dondi, M.; Lyubenova, T. S.; Carda, J. B.; Ocana, M. *J. Am. Ceram. Soc.* **2009**, *92*, 1972−1980.
(10) Dondi, M.; Matteucci, F.; Cruciani, G.; Gasparotto, G.; Tobaldi, D. M. *Solid State Sci.* **2007**, *9*, 362−369.
(11) Matteucci, F.; Cruciani, G.; Dondi, M.; Gasparotto, G.; Tobaldi, D. M. *J. Solid State Chem.* **2007**, *180*, 3196−3210.
(12) Laha, S.; Sharma, R.; Bhat, S. V.; Reddy, M. L. P.; Gopalakrishnan, J.; Natarajan, S. *Bull. Mater. Sci.* **2011**, *34*, 1257−1262.
(13) Tamilarasan, S.; Sarma, D.; Reddy, M. L. P.; Natarajan, S.; Gopalakrishnan, J. *RSC Adv.* **2013**, *3*, 3199−3202.
(14) Cooper, M. A.; Hawthorne, F. C. *Can. Mineral.* **1996**, *34*, 821−826.
(15) Hanke, K. *Naturwissenschaften* **1966**, *53*, 273.
(16) Feger, C. R.; Schimek, G. L.; Kolis, J. W. *J. Solid State Chem.* **1999**, *143*, 246−253.
(17) Larson, A. C.; Von Dreele, R. B. *General Structure Analysis System (GSAS)*, Los Alamos National Laboratory Report LAUR 86-748; Los Alamos National Laboratory: Los Alamos, NM, 2000; p 86.
(18) Giannozzi, P.; Baroni, S.; Bonini, N.; Calandra, M.; Car, R.; Cavazzoni, C.; Ceresoli, D.; Chiarotti, G. L.; Cococcioni, M.; Dabo, I.; Corso, A. D.; Gironcoli, S.; Fabris, S.; Fratesi, G.; Gebauer, R.; Gerstmann, U.; Gougoussis, C.; Kokalj, A.; Lazzeri, M.; Martin-Samos, L.; Marzari, N.; Mauri, F.; Mazzarello, R.; Paolini, S.; Pasquarello, A.; Paulatto, L.; Sbraccia, C.; Scandolo, S.; Sclauzero, G.; Seitsonen, A. P.; Smogunov, A.; Umari, P.; Wentzcovitch, R. M. *J. Phys.: Condens. Matter* **2009**, *21*, 395502(19pp).
(19) Rojo, J. M.; Mesa, J. L.; Pizarro, J. L.; Lezama, L.; Arriortua, M. I.; Rojo, T. *J. Solid State Chem.* **1997**, *132*, 107−112.
(20) Holmes, O. W.; McClure, D. S. *J. Chem. Phys.* **1957**, *26*, 1686−1694.
(21) Pascual, J. L.; Savoini, B.; Gonzalez, R. *Phys. Rev. B* **2004**, *70*, 045109−045117.